

# Nanoscale Advances

Accepted Manuscript

This article can be cited before page numbers have been issued, to do this please use: B. Zhang, S. Slavkovic, Y. Qiu, C. Peng and J. I. Chen, *Nanoscale Adv.*, 2024, DOI: 10.1039/D4NA00244J.



This is an Accepted Manuscript, which has been through the Royal Society of Chemistry peer review process and has been accepted for publication.

Accepted Manuscripts are published online shortly after acceptance, before technical editing, formatting and proof reading. Using this free service, authors can make their results available to the community, in citable form, before we publish the edited article. We will replace this Accepted Manuscript with the edited and formatted Advance Article as soon as it is available.

You can find more information about Accepted Manuscripts in the [Information for Authors](#).

Please note that technical editing may introduce minor changes to the text and/or graphics, which may alter content. The journal's standard [Terms & Conditions](#) and the [Ethical guidelines](#) still apply. In no event shall the Royal Society of Chemistry be held responsible for any errors or omissions in this Accepted Manuscript or any consequences arising from the use of any information it contains.

The data supporting this article have been included as part of the Supplementary Information.

Open Access Article. Published on 02/25/2024. Downloaded on 16/7/2567 16:33:05.  
This article is licensed under a Creative Commons Attribution-NonCommercial 3.0 Unported Licence.



# Nickel Coating on Plasmonic Copper Nanoparticles Lowers Cytotoxicity and Enables Colorimetric pH Readout for Antibacterial Wound Dressing

## Application

Bohan Zhang<sup>a</sup>, Sladjana Slavkovic<sup>a,b,c</sup>, Yumin Qiu<sup>d</sup>, Chun Peng<sup>d,e</sup>, and Jennifer I-Ling Chen<sup>a\*</sup>

a. Department of Chemistry, York University, 4700 Keele Street, Toronto, M3J 1P3, Ontario, Canada

b. Current address: Department of Laboratory Medicine, Keenan Research Centre for Biomedical Science of St. Michael's Hospital, Toronto, ON, Canada

c. Current address: Canadian Blood Services Centre for Innovation, Toronto, ON, Canada

d. Department of Biology, York University, 4700 Keele Street, Toronto, M3J 1P3, Ontario, Canada

e. Centre for Research on Biomolecular Interactions, York University, 4700 Keele Street, Toronto, M3J 1P3, Ontario, Canada

\*Email: [jlchen@yorku.ca](mailto:jlchen@yorku.ca)



**KEYWORDS:** copper nanoparticles, copper-nickel core-shell nanoparticles, wound dressings, antimicrobial, pH-responsive, plasmonics.

## Abstract

Wound infection poses a significant challenge to the natural healing process. It can impede various stages of wound healing, thereby hindering tissue regeneration and increasing the risk of systemic complications. Wound dressings emerged as a crucial option in the management of infections. Herein, we investigate fabrics coated with copper-based nanoparticles for potential wound dressing application. We synthesized copper and copper-nickel (Cu-Ni) core-shell nanoparticles via a polyol synthesis and investigated their particle growth dynamics and chemical stability. The nickel coating stabilized the nanoparticles against oxidation and dissolution, while dampening the localized surface plasmon resonance of copper. When coated on the fabrics, we found that Cu-Ni NPs were slightly less effective as antibacterial agent than Cu NPs, however the cytotoxicity of Cu-Ni NPs was significantly reduced compared to pure Cu. Additionally, we show that the discoloration of nanoparticle-coated fabrics depended on pH, thus enabling the visualization of pH levels of simulated wound fluids which can provide information on the inflammatory state of the wound. Our work contributes to the understanding of copper-based nanoparticles and their potential applications in healthcare.

## 1. Introduction

Wound infections pose a significant healthcare challenge, particularly with surgical site infection that can develop in 5–20% of post-surgery cases, leading to extended hospital stays and increased morbidity, mortality rate, and costs.<sup>1,2</sup> Wound infections can lead to life-threatening



conditions like sepsis<sup>3</sup>, while chronic wounds present further humanistic and economic burdens in healthcare. Therefore, rigorous infection prevention and timely treatment are crucial for patients' safety, and innovative solutions that merge materials science and biomedicine are sought-after.

Traditional wound infection management methods, such as wound cleansing with antiseptic solutions and sterile dressings, have been crucial in reducing infections but come with drawbacks<sup>4</sup>. The overuse or improper application of antiseptics can harm healthy tissues and impede wound healing. Of the dressings that incorporate antimicrobial agents, iodine and silver-based compounds are the common active ingredients. Iodine has broad-spectrum antimicrobial activity; however, it may cause staining and irritation at the wound site and should not be used on patients with thyroid disorders or iodine allergies. Silver exhibits high antibacterial efficacy because the released silver ions bind to proteins, cause oxidative stress via reactive oxygen species, induce structural changes in bacterial cell membranes, and inhibit DNA and RNA replication.<sup>5</sup> An example of Ag-based dressing is acticoat; however, numerous studies have elucidated the cytotoxicity of silver that can prolong healing, such that their use should be limited in duration and the wound healing progress needs to be closely monitored<sup>6,7</sup>.

As a result, there is a growing interest in other nanomaterials for antimicrobial applications. Copper is an essential trace element for human health while it is toxic to many microorganisms, including bacteria, viruses, fungi and algae<sup>8</sup>. When used as nanoparticles, the high surface area facilitates the release of copper ions which can disrupt the cellular integrity of microorganisms via the generation of reactive oxygen species, oxidation of proteins and lipids, and degradation of DNA and RNA<sup>9</sup>. In wound healing, copper has been reported to accelerate tissue regeneration and wound closure by reducing the inflammatory response, stimulating the



expression of vascular endothelial growth factor, which promotes angiogenesis within the wound<sup>10</sup>, and enhancing collagen synthesis, which helps form and repair connective tissues, skin, and blood vessels<sup>11,12</sup>. Hence, CuNPs may be a compelling choice for advanced wound care applications<sup>13</sup>.

Another fundamental interest of CuNPs is their plasmonic properties. CuNPs exhibit localized surface plasmon resonance (LSPR) arising from the collective oscillation of free electrons when excited by visible light<sup>14</sup>. The unique optical property is tunable by controlling the size and shape of nanoparticles and the local dielectric environment, thus allowing for colorimetric sensing and monitoring morphological changes to the nanoparticles<sup>15,16</sup>. Although plasmon-mediated hot electron or photothermal effect can infer antimicrobial effect, this light activation is not required in CuNPs because the main mode of action is through the released copper ions<sup>9,17</sup>. Despite the promise of the dual functionality, the low stability of CuNPs poses challenges associated with their aggregation and oxidation, which can hinder consistencies in their performance, standardization and quality control for clinical use<sup>18</sup>. It is therefore essential to address the stability issues of CuNPs for diverse healthcare applications.

Herein we investigate methods to improve the stability of colloidal CuNPs, which were synthesized via the ascorbic acid and polyol reduction route with ethylene glycol. We focus on plating CuNPs with nickel to form copper-nickel core-shell nanoparticles (Cu-Ni NPs). We evaluate the optical properties, chemical stability, antibacterial performance, and cytotoxicity of the nanoparticles in the form of coated dressing. We found that Cu-Ni NPs exhibit the desired low cytotoxicity while maintaining effective antibacterial performance. Our work may help address a critical safety aspect for potential biomedical applications of copper-based nanoparticles and make them an exciting avenue for further exploration and development.



## 2. Materials and Methods

### 2.1. Materials

Copper sulfate pentahydrate (99%) was purchased from Factory Direct Chemicals. L-ascorbic acid (reagent grade), polyvinylpyrrolidone (PVP, Mw=40000), anhydrous ethylene glycol (99.8%), TWEEN 80 and nickel (II) acetate tetrahydrate ( $\text{Ni}(\text{OCOCH}_3)_2 \cdot 4\text{H}_2\text{O}$ , 99.9% trace metals basis) and Tris(hydroxymethyl)aminomethane (TRIS) were purchased from Sigma-Aldrich. Nonwoven polyester/cellulose fabric (DURX® 570) was purchased from Berkshire Corporation. Biological reagents including dulbecco's modified eagle medium (DMEM) and penicillin-streptomycin were purchased from Gibco Inc, fetal bovine serum (FBS) was purchased from Corning Inc, Cell Counting Kit 8 (CCK-8) was purchased from Selleckchem Inc, and L-Histidine (98%) was purchased from Bioshop. All reagents were used as-is.

### 2.2 Synthesis of CuNPs

A mass of 1.5 g of PVP was dissolved in 50 mL of ethylene glycol (EG) in a round-bottom flask with magnet stirring and nitrogen gas protection. The temperature was raised to 130 °C, then 0.2346 g of L-ascorbic acid (AA) and 150 mL of 0.13 M ( $1.95 \times 10^{-5}$  mol) copper sulfate pentahydrate stock solution in EG were separately added. The solution quickly became red and was reacted for 30 min, followed by cooling in an ice bath. The CuNPs in EG can be stored for 2 weeks without a noticeable change in the LSPR or can be purified by mixing 20 mL as-synthesized solution with 15 mL 95% ethanol and centrifugated at relative centrifugal force (RCF) = 16,639 g



for 30 minutes and then dried or redispersed in anhydrous ethanol depending on subsequent experiment.

### 2.3 Synthesis of Cu-Ni NPs

A mass of 0.4 g PVP and 240  $\mu\text{L}$  of 2 M NaOH(aq) was dissolved in 20 mL ethylene glycol and heated to 196  $^{\circ}\text{C}$  under nitrogen and reflux with stirring. Then, 3 mL of 0.19 M AA and  $7.8 \times 10^{-6}$  mol of purified CuNPs (0.4 fraction of the CuNP synthesis, resuspended in 1 mL of EG) were added to the reaction solution. Finally, a 1-mL EG solution containing 0.0018 M of nickel precursor was slowly injected at 2 mL/h using a syringe pump. The solution was allowed to react for an additional 30 min.

### 2.4. Characterization of CuNPs and Cu-Ni NPs

The extinction spectra of CuNPs and Cu-Ni NPs were measured using a Lambda 950 UV/VIS/NIR spectrophotometer (Perkin Elmer). Powder x-ray diffraction was performed with an AXRD Benchtop powder x-ray diffractometer with 0.1 degree/min scan rate, 10s dwell time, and 0.1 mm slit width. Particle size and distribution of NPs were analyzed using dynamic light scattering on a Malvern Zetasizer Ultra instrument with a 0.63 mm beam diameter HeNe gas laser. The Fourier Transform Infrared spectra of PVP and CuNPs were acquired in powder form using an ATR ALPHA II Compact FT-IR Spectrometer from Bruker Inc., covering a spectral range of 4000–400  $\text{cm}^{-1}$ . The morphology and composition of the CuNPs and Cu-Ni were examined using a scanning electron microscope with the model Thermofisher Quanta 3D, operating at an accelerating potential of 10 kV, and equipped with energy dispersive x-ray analysis. Scanning transmission electron microscopy analysis was performed using a Hitachi HF-3300 TEM/STEM





equipped with a Bruker XFlash 6T160 for Energy-Dispersive X-ray Spectroscopy analyses. The microscope was operated at an accelerating voltage of 300 kV (and had an electron gun with an emission current of 17  $\mu\text{A}$ ). All measurements were performed at room temperature. The Finite-Difference Time-Domain simulation of the optical properties was carried out using Ansys Lumerical software (see supplementary information).

## 2.5. Antibacterial activity of CuNPs- and Cu-Ni NPs-coated fabrics

NP-coated fabrics were tested against the Gram-negative bacterium DH5-Alpha (BL21) *Escherichia coli* cells (*E. coli*). Japanese Industrial Standard (JIS) L 1902 antimicrobial test for textiles was implemented for quantitative analysis.

Pieces of 2 cm  $\times$  2 cm nonwoven polyester fabric were cut. These fabrics were sterilized by soaking in ethanol and then dried. Select volumes of as-synthesized NPs (e.g. 2.5, 5, 10, 15, and 20 mL corresponding to theoretical amounts of 1, 2, 4, 6 and 8  $\mu\text{mol}$  of Cu) were purified via centrifugation (RCF = 16,639 g for 30 minutes) and resuspension in anhydrous ethanol. The final concentrated NP ethanolic solution (400  $\mu\text{L}$ ) was dropped onto the surface of the fabric and the fabric was dried for 30 minutes under nitrogen. The NPs were coated on the surface of the fabric upon evaporation.

*E. coli* was incubated in fresh Luria-Bertani broth for 24 hours, and a JENWAY 6300 model spectrophotometer was used to quantify the optical density of *E. coli* to determine its concentration. Then, 200  $\mu\text{L}$  of cultured *E. coli* with a concentration between  $1 \times 10^5$  and  $3 \times 10^5$  cells/mL was added onto NPs-coated fabric using a micropipette. The fabric was placed inside a 50 mL Falcon tube in an oven at 37  $^\circ\text{C}$  and incubated for 18 hours. After incubation, the *E. coli*



was rinsed off the fabric using 40  $\mu$ L of Tween 80 and 20 mL of 0.9% NaCl solution with vortexing for 30 seconds. The count of bacterial colonies was carried out via the serial dilution plate count method using a 0.9% NaCl solution after a one-day incubation period on the agar plate surface.

Antibacterial properties were quantified by calculating bacterial colony reduction rate (antibacterial activity), which is defined as:

$$\text{Antibacterial activity} = \frac{T_0 (\text{untreated}) - T_{18\text{h}} (\text{treated})}{T_0 (\text{untreated})} \times 100\%$$

Additional quantitative analyses according to JIS L 1902/2008<sup>19</sup> are in supplementary information.

## 2.6. Cytotoxicity assays of CuNPs- and Cu-Ni NPs-coated fabrics

For the cytotoxicity assessment, BJ (ATCC CRL-2522) fibroblast cells were employed. Specifically, 6,000 cells/well BJ cells were seeded in 96-well plates and cultured in 100  $\mu$ L of DMEM containing 20% FBS overnight. Concurrently, 6  $\mu$ mol of CuNPs or Cu-Ni NPs were applied as coatings on 2 cm  $\times$  2 cm non-woven fabric substrates. Each piece of NP-coated fabric was immersed in 1 mL of phosphate-buffered saline (PBS) containing 1% penicillin-streptomycin for an 18-hour incubation period at room temperature. Then, the specified volumes of the resulting extracts were mixed with DMEM supplemented with 20% FBS to a final volume of 100  $\mu$ L. This mixture was subsequently added to individual wells of the 96-well plate, each initially containing 6,000 BJ cells. The cells were subsequently incubated at 37  $^{\circ}$ C with a 5% CO<sub>2</sub> atmosphere for 2 days.

After the 2-day incubation period, cell viability was determined using the a Cell Counting Kit 8 (CCK-8) kit following manufacturer's suggested protocols. Briefly, 10  $\mu$ L of the CCK-8



solution was added into each well and cells were incubated with the CCK-8 solution for 2 hours. During this incubation, viable cells with cellular dehydrogenases reduced the WST-8 dye within the CCK-8 solution, forming formazan and a color change from colorless or pale yellow to orange. The optical density (OD) of the CCK-8 solution was measured at 450 nm using an Agilent BioTek Synergy H4 hybrid microplate reader. Cell viability (CV) was calculated as follows:

$$CV(\%) = \frac{[A(\text{NPs}^+) - A(\text{Blank})]}{[A(\text{NPs}^-) - A(\text{Blank})]} \times 100\%$$

where A(NPs+) is the OD value of well with cells and NP-coated fabric extract; A(NPs-) is the OD value of well with cells without NP-coated fabric extract; A(Blank) is the OD value of wells with culture medium, but without cells.

The OD of BJ cells incubated with NP-fabric extract was compared to control cells (i.e. without NP-fabric extracts) to yield CV as a percentage. A high percentage of CV suggests greater cell viability, indicating the NP-coated fabric that is used to incubate with BJ cells has low cytotoxicity.

## 2.7. Simulated wound exudate on nanoparticle-coated fabric

A simulated wound exudate (SWE) was formulated by combining 0.142 M NaCl and 0.0025 M CaCl<sub>2</sub>·2H<sub>2</sub>O, with pH buffering agents including 0.025 M TRIS and 0.005 M L-Histidine. The SWE was prepared at three different pHs: 3.5, 7, and 10. The fabrics coated with 6 μmol of CuNPs or Cu-Ni NPs were separately soaked in 3 mL of SWE for 105 minutes.

## 2.8. Statistical Analysis



Cytotoxic effects were analyzed using the Student's t-test to compare mean cell viability levels across groups. The differences were statistically significant at  $p < 0.05$ . Data were reported as mean  $\pm$  standard error.

### 3. Result and discussion

We synthesized CuNPs via polyol reduction.<sup>20</sup> The EG solution with AA and PVP were heated to 130 °C under N<sub>2</sub>. The CuSO<sub>4</sub> stock solution was rapidly added, turning the solution red in 22 s. Figure 1a shows the UV-vis extinction spectrum of as-synthesized CuNPs with a sharp LSPR peak centered at 584 nm and a relatively low baseline at long wavelengths (>800 nm), suggesting that the CuNPs were dispersed with minimal aggregation. The LSPR peak wavelength agrees with theoretical simulation using the Finite-difference time-domain (FDTD) method for CuNPs (Figure S1). The scanning electron microscope (SEM) image in Figure 1b shows that the CuNPs were predominantly spherical with an average diameter of  $76.4 \pm 15.3$  nm; the distribution of the particle size is shown in Figure 1c. Powder x-ray diffraction (PXRD) shown in Figure 1d, collected using a cell holder sealed under nitrogen to limit oxidation, confirms the metallic phase of the CuNPs with diffraction peaks at  $2\theta$  values of 43.2°, 50.4°, and 74.1°, corresponding to the (111), (200), and (220) crystallographic planes of copper of space group *fm-3m*. The calculated crystallite size of the CuNPs was 14.7 nm using the Scherrer equation (see Supplementary Information), suggesting that CuNPs are polycrystalline.



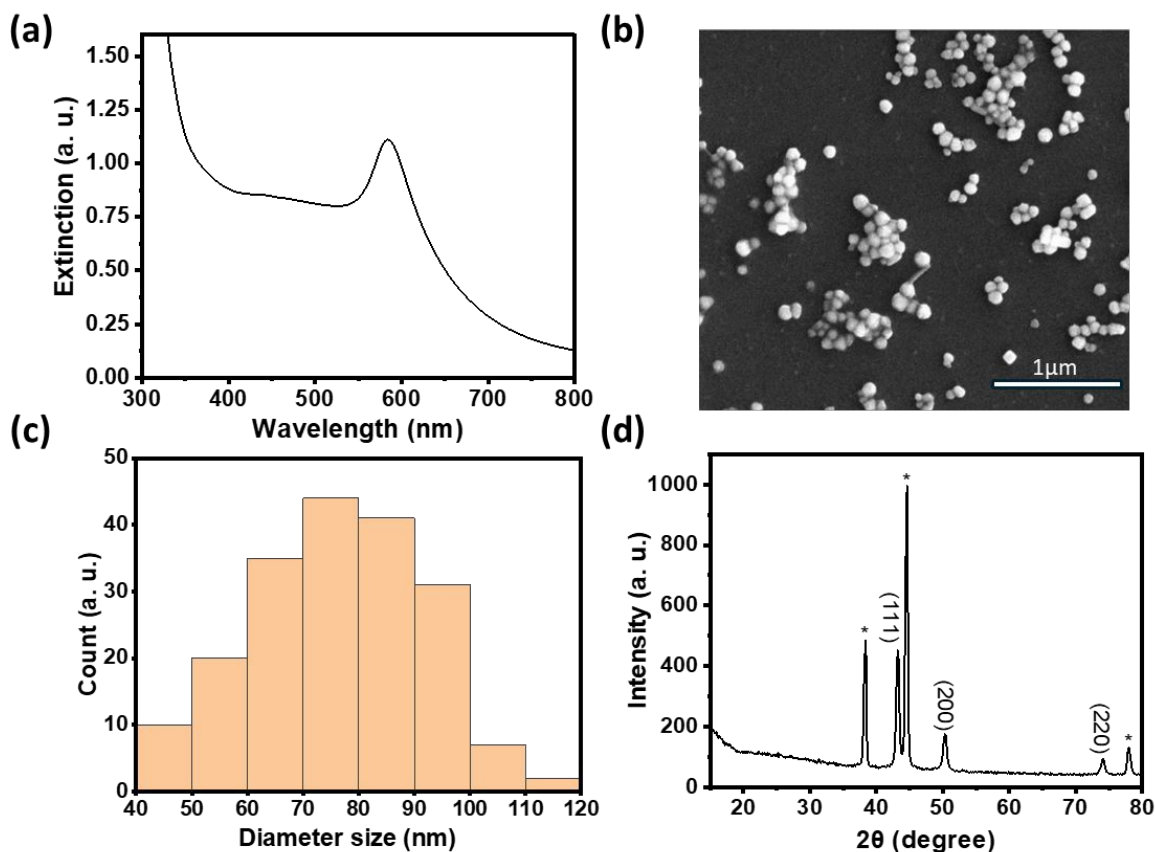


**Figure 1.** (a) UV-vis extinction spectrum of as-synthesized CuNPs. (b) SEM image of CuNPs and (c) their size distribution (N=175). (d) XRD pattern of purified CuNPs (peaks labeled with \* came from the sample holder).

We examined the evolution of the nanoparticle growth during the reaction by monitoring the UV-vis extinction spectra (Fig. 2a) and dynamic light scattering (DLS) properties (Fig. 2b) over time. We observed an initial blueshift followed by increasing intensity in the LSPR peak. At the shortest time (22 s), the Cu nuclei or atoms were aggregated and clustered as detected in DLS. As the synthesis progressed, the CuNPs became dispersed and the hydrodynamic size decreased from  $107.4 \pm 4.8$  to  $87.8 \pm 3.1$  nm (Table S1). The observed initial blue shift in the LSPR peak during the synthesis of CuNPs aligns with the concurrent decrease in size, as determined by DLS



analysis. The increase in the intensity of the LSPR peak thereafter indicates a rise in the concentration of CuNPs while the size remained the same.

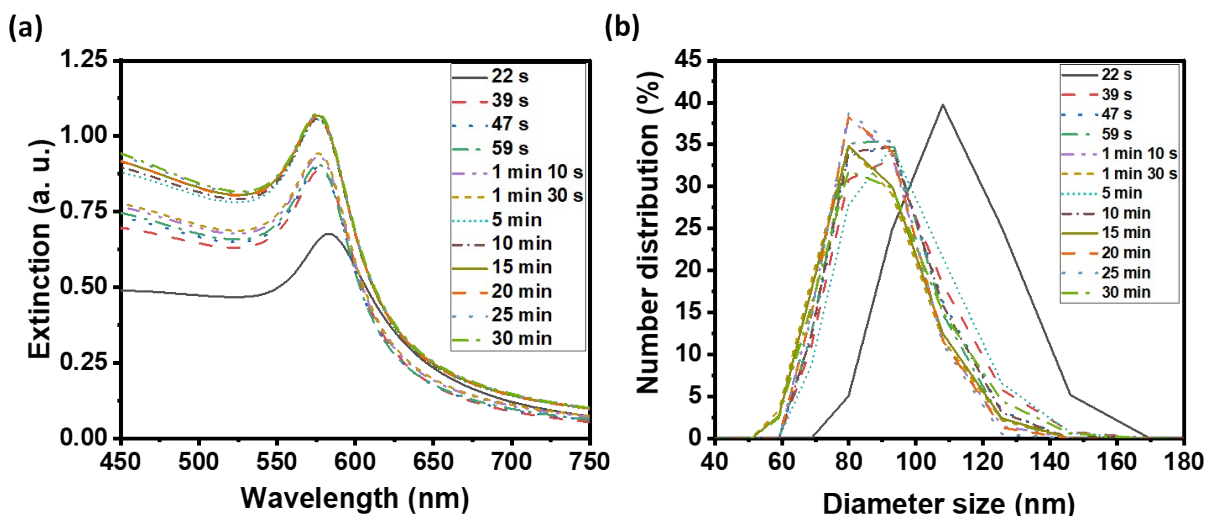


**Figure 2.** (a) UV-visible extinction spectra of as-synthesized CuNPs solution, and (b) distribution of CuNPs hydrodynamic diameter by DLS at various reaction times.

In the synthesis, we utilized PVP as a capping agent, which helped increase the stability of CuNPs by preventing aggregation, controlling the particle size and shape, and providing a protective coating on the nanoparticle surface. The reducing agent, AA, can also act as a capping agent to stabilize the CuNPs. However, the FT-IR spectrum in Figure S2 shows that the CuNPs were mainly capped with PVP, where the stretching vibrational modes of C=O and C-N were observed at  $1650\text{ cm}^{-1}$  and  $1269\text{ cm}^{-1}$ , respectively, and that of C-H and N-H were observed at  $2800\text{--}3000\text{ cm}^{-1}$  and  $3100\text{--}3500\text{ cm}^{-1}$ , respectively.

It is critical to enhance the chemical stability of CuNPs due to their susceptibility to oxidation. While the as-synthesized CuNPs were stable in EG for an extended period of time, they



oxidized upon purification and redispersion in aqueous or ethanolic solutions. Improving the chemical stability will prolong the duration of Cu ion release, thereby enhancing antimicrobial properties. The LSPR of CuNPs allows for facile monitoring of the changes and dissolution of the CuNPs spectroscopically. We first examined the incorporation of excess organic ligands and capping agents, such as AA and PVP, to improve the chemical stability of CuNPs. Figure S3 shows the changes in the LSPR peak of CuNPs redispersed in water with the additives. Some improvements were seen with the addition of AA or PVP; however, they were ineffective as the LSPR peak of CuNPs rapidly decreased to 60% of the original intensity within 200 minutes for the most promising trial (Figure S3a-b). Motivated by cupronickel, a blend of copper and nickel in varying proportions that forms durable alloys with excellent corrosion resistance and are used in medical devices,<sup>21</sup> we then explored Ni coating to increase the chemical stability of CuNPs. We hypothesized that Ni coating can reduce the oxidation and dissolution of copper and enable prolonged copper ion release, thereby addressing the limitations of copper-based nanoparticles<sup>22</sup>.

In comparison to copper, nickel has a much lower reduction potential<sup>23,24</sup>. We first investigated the feasibility of reducing various Ni (II) compounds in the polyol synthesis by increasing the temperature to 196 °C to increase the reducing power. Interestingly, PXRD data in Figure 3a shows that metallic Ni was readily formed with nickel acetate as the precursor while a mixture of metallic Ni and various Ni hydroxides was formed when nickel sulfate was used as the precursor<sup>25</sup>. Previous work examining the polyol reduction mechanism reported metal glycolates as the intermediate species from metal salts like sulfate and chloride<sup>26,27</sup>. We hypothesize that nickel acetate remained as a complex and may be more easily reduced to Ni (0), hence minimizing the formation of by-products like nickel hydroxide.



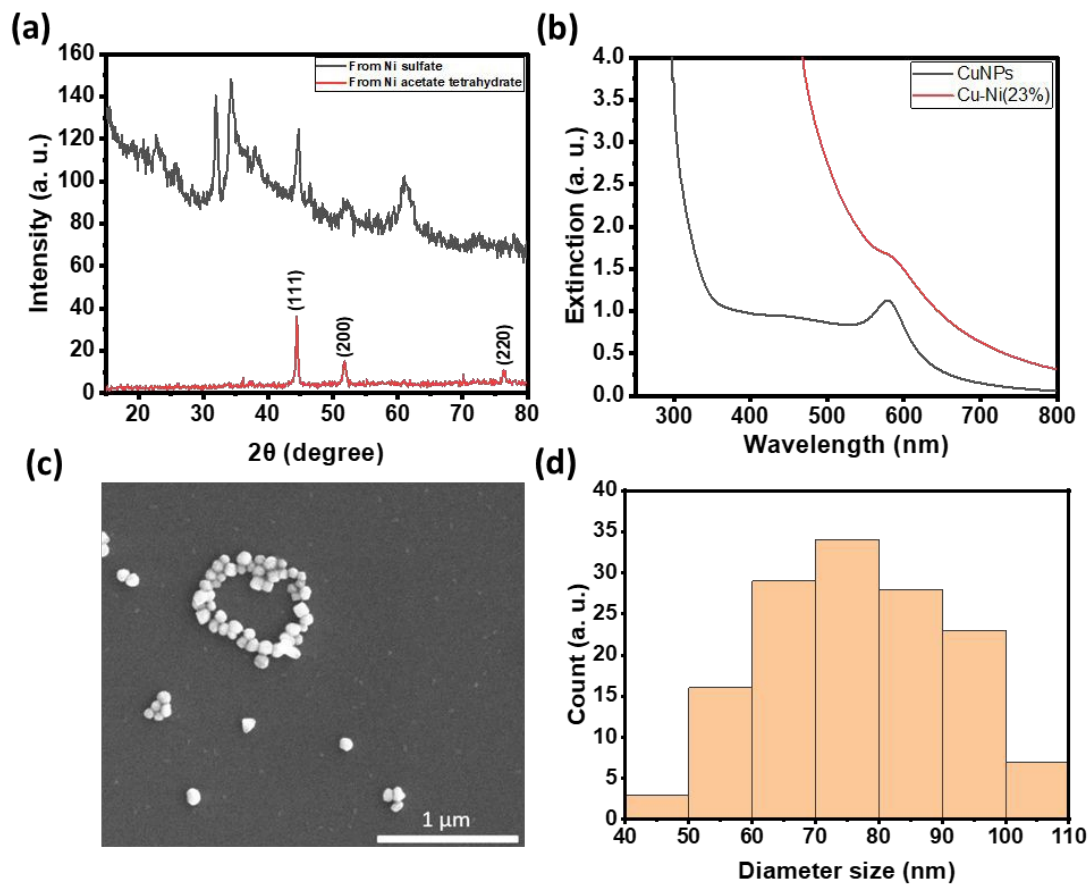


**Figure 3.** (a) X-ray diffraction patterns of metallic nickel synthesized from nickel acetate tetrahydrate (top red) and mixed nickel hydroxide and oxide from nickel sulfate (bottom black). (b) UV-vis extinction spectrum of as-synthesized CuNPs and Cu-Ni NPs. (c) SEM image of Cu-Ni NPs and (d) their size distribution (N=126).

We thus used nickel acetate as the precursor to incorporate a nickel shell on the CuNPs. The synthesis comprised two steps: first, CuNPs were synthesized, purified and redispersed in ethylene glycol growth solution, and then nickel precursor was slowly added. We found that the addition of a small amount of NaOH to be critical in keeping the colloidal stability of CuNPs at 196 °C; it may help with the electrostatic repulsion between negatively charged hydroxylated





CuNPs. We examined Ni loadings of 23, 62, 94, and 154 mol% (Figure S3c); however, only that of 23 mol% yielded nanoparticles that can be centrifuged and purified. We denote them as Cu-Ni NPs. During the shell growth, the solution turned from red to dark brown, and the purified Cu-Ni NPs were black in colour. The Cu-Ni NPs exhibited a weaker LSPR as seen in the extinction spectrum in Figure 3b, consistent with theoretical simulation (Fig. S1), because Ni is not plasmonic and causes an overall dampening. The average size of Cu-Ni NPs was  $77.3 \pm 14.6$  nm, similar to that of CuNPs. Figure 4 shows scanning transmission electron microscopy (STEM) images of Cu-Ni NPs and their elemental mapping, which confirms the deposition of Ni on Cu (red and cyan, respectively in Fig 4b, d) and the core-shell structure. On the other hand, the atomic % of Ni to Cu from energy-dispersive x-ray spectroscopy (EDS) analysis was much lower than the theoretical composition (1.6 mol% vs 23 mol%). The discrepancy may be attributed to factors such as the incomplete reduction of the nickel precursor or the mismatch in the lattice and structure between the surface hydroxylated CuNPs and metallic Ni. Although Ni dampens the LSPR, the weak plasmonic peak was still seen and was used to monitor the stability of Cu-Ni NPs. Figure S4a, b shows extinction spectra of CuNPs and Cu-Ni NPs redispersed in ethanol over time; after 250 minutes, the LSPR peak intensity remained at 80 % for Cu-Ni NPs compared with CuNPs at 55 %. The Ni coating also yielded better stability enhancement than excess AA or PVP.



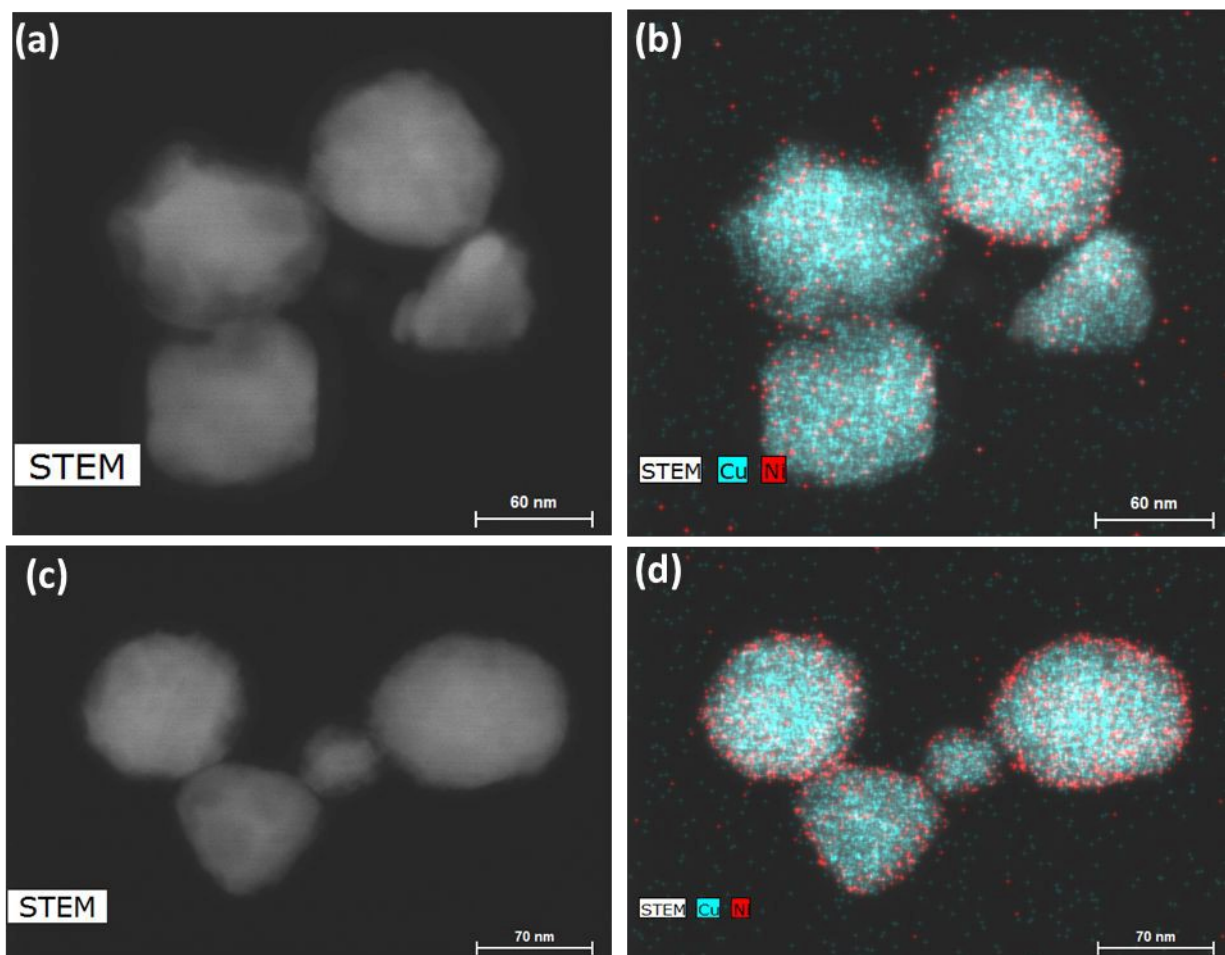


**Figure 4.** (a,c) STEM images and (b,d) elemental mapping of Cu-Ni nanoparticles. Cu and Ni are shown, respectively, as cyan and red. The EDS atomic ratio of Ni:Cu was 1.6:100.

For antibacterial and cytotoxicity analyses, we coated non-woven polyester textiles with varying loadings of CuNP or Cu-Ni NP. The colloidal particles were physisorbed onto the textiles after drying under nitrogen. Figure 5c shows the photographs of CuNP- and Cu-Ni NP-coated fabrics. There was negligible loss of CuNPs or Cu-Ni NPs from the polyester fabric from rinsing, but some can be removed by sonication or when vigorously shaken in solution.

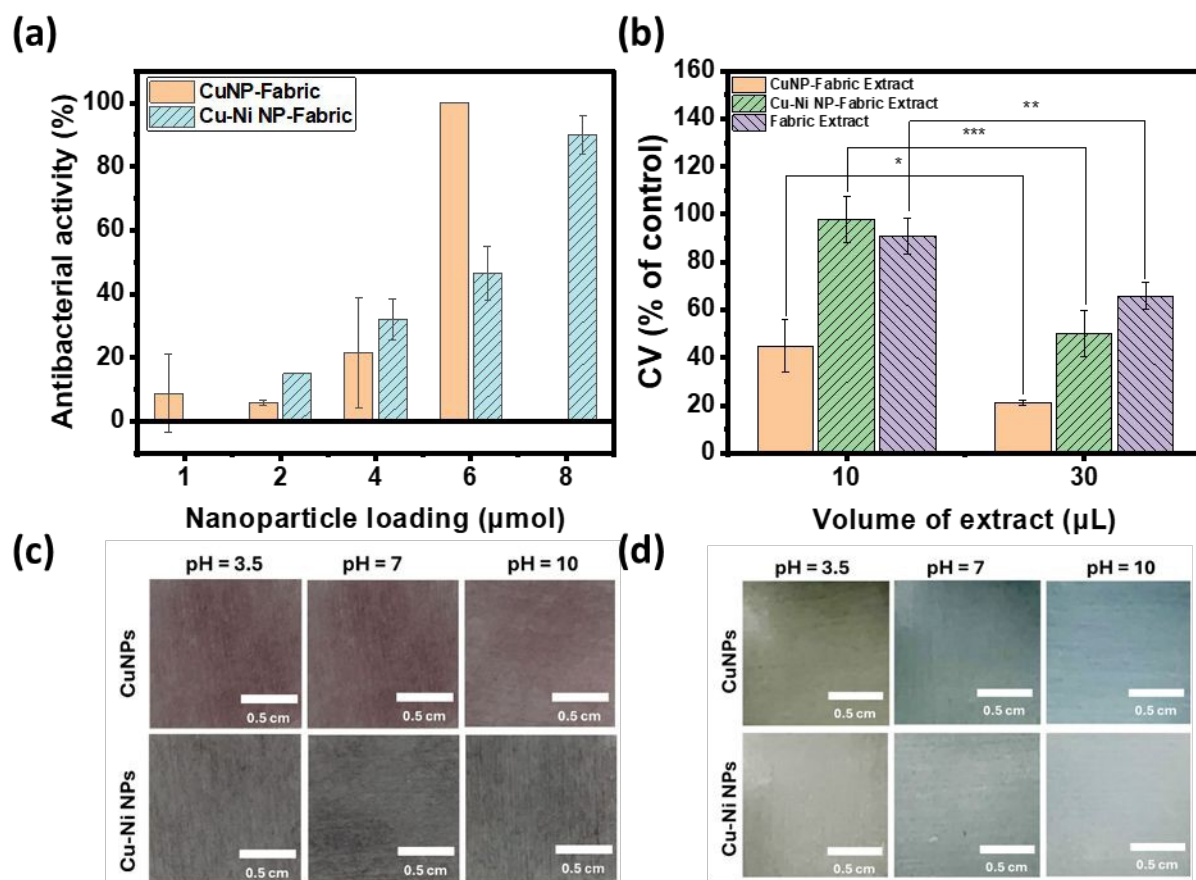


Figure 5a summarizes the number of colonies of *E. coli* recovered from the NP-coated fabrics at different NP loading. We observed a reduction in bacterial colonies with increasing amounts of CuNPs and Cu-Ni NPs on the fabrics. At 6  $\mu\text{mol}$ , a remarkable decrease of up to  $99.98 \pm 0.04$  % in *E. coli* colony count was recorded for CuNP-coated fabric samples; in comparison, a decrease of up to  $90.03 \pm 6.04$  % was achieved for Cu-Ni NP loading of 8  $\mu\text{mol}$ . The higher loading of Cu-Ni NP required may be related to the slower release of copper ions. We summarized bacteriostatic (BS) and bactericidal (BC) values in Table S2. The results show that CuNP loading of  $>6$   $\mu\text{mol}$  (i.e.  $1.5$   $\mu\text{mol}\cdot\text{cm}^{-2}$ ) on fabrics was effective at both prohibiting the growth and killing *E. coli*, based on the certification standards of antibacterial finished textile products<sup>28</sup>. Although the minimum loading of Cu-Ni NP required to meet certification standards is higher, Cu-Ni NP loading may retain the antibacterial properties for a longer period of time.

For wound dressing applications, it is desirable to have antimicrobial efficacy while exhibiting low cytotoxicity. Hence, we carried out cytotoxicity studies of extracts from CuNP- and Cu-Ni NP-coated fabrics on a model human fibroblast - BJ cells. Figure 5b compares the viability of cells incubated with 10 or 30  $\mu\text{L}$  extracts of CuNP- and Cu-Ni NP-coated fabrics and those of control, i.e. cells incubated with extracts of non-coated fabric and cultured in DMEM. We observed that an increase in the volume of the extracts (30  $\mu\text{L}$  vs 10  $\mu\text{L}$ ) resulted in a decrease in cell survival rates across all samples. The extracts of CuNP-coated fabric exhibited significant toxicity to BJ cells, with cell viability (CV) of  $44.8 \pm 11.1$  and  $21.2 \pm 1.0$  % was determined for 10  $\mu\text{L}$  and 30  $\mu\text{L}$  samples respectively. The extracts of Cu-Ni NP-coated fabric exhibited much lower cytotoxicity, as evidenced by a higher average CV at  $97.9 \pm 9.9$  and  $50.0 \pm 9.7$  % for 10  $\mu\text{L}$  and 30  $\mu\text{L}$  of extracts, respectively. The extracts of the control - namely PBS incubated with non-



coated fabric - showed some effect on cell viability as the growth media was diluted. Notably, the extracts from Cu-Ni NP-coated fabric yielded statistically the same results as the control at 10  $\mu\text{L}$  volume (at  $p > 0.4$ ). The low cytotoxicity of Cu-Ni NPs suggests a better biocompatibility than CuNPs.



**Figure 5.** (a) Antibacterial activity of different amounts of CuNP- or Cu-Ni NP-coated fabrics. (b) Cell viability after incubation with extracts of CuNP- and Cu-Ni NP-coated fabrics. \*:  $p < 0.05$ . \*\*:  $p < 0.01$ . \*\*\*:  $p < 0.001$ . Photographs of CuNP- and Cu-Ni NP-coated fabrics in SWE with different pHs c) at the beginning and d) after 105 min of incubation.



Lastly, we examined the colorimetric response of the NP-coated fabrics to SWE at different pHs. Wound exudate comprising plasma, proteins, and white blood cells is vital for healing by providing nutrients and facilitating debris removal. Bacterial infections can raise the pH of the exudate, thereby negatively impacting the healing process<sup>29</sup>. Therefore, it would be advantageous if a wound dressing could provide a visual cue to the state of the infection.

Figure 5c and 5d show the photographs of CuNP- (top) and Cu-Ni NP- (bottom) coated fabrics in SWE with pH= 3.5, 7, and 10 (from left to right) at time 0 and after 105 minutes. After 105 minutes, the color of the CuNP- and Cu-Ni NP-coated fabrics turned orange/yellow in SWE of pH 3.5, which may be attributed to residual CuNPs and the formation of copper (I) oxide at acidic pH. In neutral or alkaline SWE, the NP-coated fabrics turned blue, and species such as Cu (II) hydroxide or other adsorbed Cu<sup>2+</sup> complexes may contribute to the observed color change. The colors darkened and persisted after one month (Fig. S5). Those results show that CuNP- and Cu-Ni NP-coated fabrics not only combat bacterial infections but also provide a colorimetric response to pH. Since normal exudate usually has an acidic pH ranging from 4 to 6<sup>30</sup>, the color change to blue could point to an alkaline environment that may be associated with bacterial infection. Hence copper-based NPs may enable a diagnostic element to wound care without additional sensor technology integration.

## 4. Conclusions

We showed that copper nanoparticles with known antibacterial properties can be stabilized by plating a nickel shell. These copper-based nanoparticles exhibit localized surface plasmon resonance that provides a colorimetric handle to visually detect changes in their size and



dissolution, such as in response to pH changes in wound exudates. Although installing a nickel shell decreased slightly the antibacterial efficacy, the resultant Cu-Ni NPs were significantly less cytotoxic than pure CuNPs – an important attribute of infection-control agents. Further studies on different compositions of Cu-Ni NPs, their large-scale production, and antimicrobial performance against a variety of species will help elucidate the feasibility of their use in healthcare.

## Author contributions

BZ carried out all experimental work and data analyses. SS designed antibacterial testing methodology and YQ and CP supported cytotoxicity measurement. JC conceptualized the project and provided supervision. BZ and JC wrote the manuscript with input and approval from all authors. Funding was secured by JC and CP.

## 5. Conflicts of interest

The authors declare no financial or non-financial conflicts of interest that could influence the objectivity or integrity of the presented research.

## 6. Acknowledgements

This research was supported by York University's COVID-19 rapid research fund, and NSERC Research Tool and Instruments, and Discovery grants to JILC and a CIHR project grant (PJT-166079) to CP. We thank Dr. Jaklewicz and Dr. Nikbin at York University and University of Toronto, respectively, for technical support on EM imaging and Prof. Johnson for use of facility for bacterial work.

## 7. Footnotes



Electronic Supplementary Information (ESI) available: Additional experimental details and calculations, FDTD simulations, SEM, FT-IR, UV-vis spectra, DLS and quantitative antibacterial test and method. See DOI:



## 8. References

- 1 B. M. Andersen, in *Prevention and Control of Infections in Hospitals*, Springer International Publishing, 2019, pp. 377–437.
- 2 J. M. Badia, A. L. Casey, N. Petrosillo, P. M. Hudson, S. A. Mitchell and C. Crosby, *J. Hosp. Infect.*, 2017, **96**, 1–15.
- 3 C. K. Sen, *Adv Wound Care (New Rochelle)*, 2021, **10**, 281–292.
- 4 I. B. M. Ploegmakers, S. W. M. Olde Damink and S. O. Breukink, *Br. J. Surg.*, 2017, **104**, e24–e33.
- 5 A. Muhammad, in *Nanomedicines*, ed. N. Ivanova, V. Gugleva, M. Dobрева, I. Pehlivanov, S. Stefanov and V. Andonova, IntechOpen, London, 1st edn, 2018, vol 5, ch.4, pp. 71-92.
- 6 K. Nešporová, V. Pavlík, B. Šafránková, H. Vágnerová, P. Odrážka, O. Židek, N. Císařová, S. Skoroplyas, L. Kubala and V. Velebný, *Sci Rep*, 2020, **10**, 15216.
- 7 A. Burd, C. H. Kwok, S. C. Hung, H. S. Chan, H. Gu, W. K. Lam and L. Huang, *Wound Repair Regen*, 2007, **15**, 94–104.
- 8 N. Cioffi and M. Rai, in *Nano-Antimicrobials: Progress and Prospects*, ed. D. Longano, N. Ditaranto, L. Sabbatini, L. Torsi and N. Cioffi, Springer-Verlag, Berlin Heidelberg, 1st edn, 2014, ch.3, pp. 85–117.
- 9 A. K. Chatterjee, R. Chakraborty and T. Basu, *Nanotechnology*, 2014, **13**, 135101.
- 10 C. K. Sen, S. Khanna, M. Venojarvi, P. Trikha, E. Christopher Ellison, T. K. Hunt and S. Roy, *Am J Physiol Heart Circ Physiol*, 2002, **5**, H1821-H1827.





- 11 S. K. Nethi, S. Das, C. R. Patra and S. Mukherjee, *Biomater Sci*, 2019, **7**, 2652–2674.
- 12 A. P. Kornblatt, V. G. Nicoletti and A. Travaglia, *J Inorg Biochem*, 2016, **161**, 1–8.
- 13 G. Borkow, J. Gabbay, R. Dardik, A. I. Eidelman, Y. Lavie, Y. Grunfeld, S. Ikher, M. Huszar, R. C. Zatcoff and M. Marikovsky, *Wound Repair Regen*, 2010, **18**, 266–275.
- 14 F. Parveen, B. Sannakki, M. V. Mandke and H. M. Pathan, *Sol. Energy Mater. Sol. Cells*, 2016, **144**, 371–382.
- 15 J. Boken, P. Khurana, S. Thatai, D. Kumar and S. Prasad, *Appl Spectrosc Rev*, 2017, **52**, 774–820.
- 16 K. A. Willets and R. P. Van Duyne, *Annu Rev Phys Chem*, 2007, **58**, 267–297.
- 17 A. D’Agostino, A. Taglietti, R. Desando, M. Bini, M. Patrini, G. Dacarro, L. Cucca, P. Pallavicini and P. Grisoli, *Nanomaterials*, 2017, **1**, 7.
- 18 R. L. Calabro, F. J. Burpo, S. F. Bartolucci and J. A. Maurer, *J. Phys. Chem. C*, 2023, **127**, 15307–15315.
- 19 Japanese Standards Association, *Testing for Antibacterial Activity and Efficacy on Textile Products. Jis L 1902:2008*, Japanese Standards Association, Tokyo, 2009.
- 20 F. Fievet, S. Ammar-Merah, R. Brayner, F. Chau, M. Giraud, F. Mammeri, J. Peron, J. Y. Piquemal, L. Sicard and G. Viau, *Chem Soc Rev*, 2018, **47**, 5187–5233.
- 21 M. S. Parvizi, A. Aladjem and J. E. Castle, *Int. Mater. Rev.*, 1988, **33**, 169–200.



- 22 S. Zhao, F. Han, J. Li, X. Meng, W. Huang, D. Cao, G. Zhang, R. Sun and C. Wong, *Small*, 2018, **14**, 1800047.
- 23 G. Milazzo, S. Caroli and R. D. Braun, *J Electrochem Soc*, 1978, **125**, 261C.
- 24 A. Bard, R. Parsons and J. Jordan, *Standard potentials in aqueous solution*, Routledge, London, 2017.
- 25 D. S. Hall, D. J. Lockwood, C. Bock and B. R. MacDougall, *Proc. R. Soc. A*, 2015, **471**, 20140792.
- 26 K. J. Carroll, J. U. Reveles, M. D. Shultz, S. N. Khanna and E. E. Carpenter, *J. Phys. Chem. C*, 2011, **115**, 2656–2664.
- 27 K. Takahashi, S. Yokoyama, T. Matsumoto, J. L. C. Huaman, H. Kaneko, J.-Y. Piquemal, H. Miyamura and J. Balachandran, *New J. Chem*, 2016, **40**, 8632–8642.
- 28 Japan Textile Evaluation Technology Council, *JEC301. The Certification Standards of Antibacterial Finished Textile Products*, Japan Textile Evaluation Technology Council, Osaka, 2012.
- 29 H. H. Leveen, G. Falk, B. Borek, C. Diaz, Y. Lynfield, B. J. Wynkoop, G. A. Mabunda, J. L. Rubricius and G. C. Christoudias, *Ann. Surg*, 1973, **6**, 745.
- 30 T. R. Dargaville, B. L. Farrugia, J. A. Broadbent, S. Pace, Z. Upton and N. H. Voelcker, *Biosens. Bioelectron*, 2013, **41**, 30–42.

